Effect of scatterer interactions on photon transport in diffusing wave spectroscopy

Nicholas Sbalbi, Qi Li, and Eric M. Furst

Phys. Rev. E **106**, 064609 — Published 16 December 2022

DOI: 10.1103/PhysRevE.106.064609

Effect of scatterer interactions on photon transport in diffusing wave spectroscopy

Nicholas Sbalbi,[1,*] Qi Li,[1] and Eric M. Furst[1,†]

[1] *Department of Chemical and Biomolecular Engineering, Allan P. Colburn Laboratory, University of Delaware, 150 Academy Street, Newark, Delaware 19716, United States*

(Dated: October 7, 2022)

We calculate the effect of particle size, concentration, and interactions on the photon transport mean free path l^* that characterizes the multiple light scattering in diffusing wave spectroscopy (DWS). For scatterers of sufficient size, such that the first peak of the suspension structure factor $S(q_{\max})$ remains in the range of accessible scattering vectors, neither repulsive nor attractive interactions between scatterers contribute strongly to l^*; its values are bounded by those for hard spheres and scatterers without interactions. However, for scatterers smaller than the wavelength of light, crowding induced by attraction or repulsion can lead to non-monotonic behavior in l^* with increasing scatterer concentration. The effect is strongest for repulsive particles.

I. INTRODUCTION

Diffusing wave spectroscopy (DWS) measures dynamics by light scattering in a high multiple-scattering regime [1, 2]. It is a non-invasive method to study soft materials, and has been widely used in academic and industrial research, including studies of colloid [3–9] and polymer solution dynamics [10, 11], protein aggregation kinetics [12, 13], drug stability [14, 15], film drying [16], microrheology [17–19], and for performing rheometry in special or extreme conditions, such as at high pressure [20, 21].

In DWS, the homodyne intensity correlation function of the light intensity $g_{(2)}(t) = \langle I(t_0)I(t_0+t)\rangle/\langle I\rangle^2$ depends on *both* the motion of the scatterers and the characteristics of light transport through the sample. It is necessary to separate these contributions to isolate, for instance, the changes in dynamics that occur when scatterers become more concentrated or interact from concurrent changes in the photon transport through the sample. In models of light transport that are used to interpret DWS measurements, the principal quantity of interest that characterizes the multiple scattering is the transport or photon mean free path length, l^*, the length over which a photon's propagation direction randomizes.

l^* depends on the spatial distribution of scatterers and their scattering characteristics. To date, there has not been a systematic calculation of l^* reported with the aim of understanding its dependence on the interactions between scatterers. Such interactions affect the spatial distribution of scatterers through a structure factor $S(q)$ and may complicate the interpretation of DWS experiments by obscuring the contributions of scatterer dynamics from those of the light transport. For instance, an increase in l^* will lead to a slower decay of the correlation function, which could be interpreted naively as slower scatter dynamics due to particle concentration or interparticle interactions.

In the present work, we calculate l^* for scatterers with increasing concentration using four model interactions: the limit of no interactions; hard spheres; repulsion modeled by an effective hard sphere; and attractive, sticky hard spheres. For scatterers of sufficient size, such that the first peak of $S(q_{\max})$ remains in the range $0 \leq q_{\max} \leq 2k_0$, neither repulsive nor attractive interactions between scatterers contribute strongly to l^*; its values are bounded by those for hard spheres and scatterers without interactions, which differ by only a small amount. Here, $k_0 = 4\pi n_s/\lambda$ for the vacuum wavelength λ and suspending medium refractive index n_s. However, for smaller scatterers, crowding induced by attraction, and espeically repulsion pushes, $q_{\max} > 2k_0$, and can lead to strong non-monotonic behavior in l^* with increasing concentration.

Before discussing the results of our calculations, we review the light transport in DWS experiments in the next section.

II. THEORY

In this section we provide an overview of the equations and methods used to calculate the photon mean-free path length, l^*. Based on the definition equation of l^*, the calculation consists of modular components that calculate the form factor, $P(q)$, and structure factor, $S(q)$. The modular structure is applied in the Python package [22] (details are in appendix C).

A. Photon mean-free path

In the photon diffusion model of multiple scattering, both the scattering mean-free path, l, and the photon mean-free path, l^*, determine the light transport proper-

* Current address: Department of Chemical Engineering, Massachusetts Institute of Technology, Cambridge, Massachusetts 02139, United States

† Corresponding author. furst@udel.edu

ties. The two are related by

$$l^* = \frac{2k_0^2}{\langle q^2 \rangle} l \tag{1}$$

where $q = 2k_0 \sin(\theta/2)$ is the scattering vector for a scattering angle θ, and $\langle \cdots \rangle$ denotes the average over all scattering angles. The scattering mean-free path is the average distance between scattering events and is given by $l = 1/\rho\sigma$, where ρ is the number density of scatterers and σ is the scattering cross section. Substituting this relation gives

$$l^* = \frac{2k_0^2}{\rho\sigma\langle q^2 \rangle} \tag{2}$$

For uniform, spherical, interacting particles,

$$\sigma = \frac{1}{k_0^2} \int_{4\pi} P(q) S(q) \mathrm{d}\Omega \tag{3}$$

where the integral is over the solid angle Ω. The average mean square scattering vector can thus be written as,

$$\langle q^2 \rangle = \frac{\int_{4\pi} q^2 P(q) S(q) \mathrm{d}\Omega}{\int_{4\pi} P(q) S(q) \mathrm{d}\Omega} \tag{4}$$

Substituting and simplifying,

$$l^* = 2k_0^4 \left(\rho \int_{4\pi} q^2 P(q) S(q) \mathrm{d}\Omega \right)^{-1} \tag{5}$$

and integrating over the azimuthal angle gives

$$l^* = k_0^4 \left(\pi\rho \int_0^{\pi} q^2 P(q) S(q) \sin\theta \mathrm{d}\theta \right)^{-1} \tag{6}$$

or, equivalently,

$$l^* = k_0^6 \left(\pi\rho \int_0^{2k_0} q^3 P(q) S(q) \mathrm{d}q \right)^{-1} \tag{7}$$

Finally, non-dimensionalizing the scattering vector with the scatterer radius a, we arrive at

$$l^* = k_0^6 a^4 \left(\pi\rho \int_0^{2k_0 a} (qa)^3 P(qa) S(qa) \mathrm{d}(qa) \right)^{-1} \tag{8}$$

The strong weighting toward high scattering vectors is an important characteristic of eqn. 8. A detailed derivation is provided by Weitz and Pine [2].

The notation for the form factor in the literature can be confusing. $P(qa)$ is *not* a normalized form factor $\tilde{P}(q)$. Therefore, the dependence of eqn. 8 on the scatterer size must also account for contributions in $P(qa)$. The two are related by

$$P(qa) = \frac{2}{9} k_0^6 a^6 \left(m-1\right)^2 \tilde{P}(qa) \tag{9}$$

where $m = n_p/n_s$ is the ratio of the particle and solvent refractive indices. Using the normalized form factor, eqn. 8 is written

$$l^* = 2(m-1)^2 \left(9\pi a^2 \rho \int_0^{2k_0 a} (qa)^3 \tilde{P}(qa) S(qa) \mathrm{d}(qa) \right)^{-1} \tag{10}$$

Equation 10 is strictly valid when the structural correlations of the dispersed scatterers occur on length scales that are smaller than l^* [23]. In this work, this condition is always true (e.g. $l^* \gg 2a$), but scatterers with significantly higher refractive index contrast (e.g. titania or zinc oxide in water) could violate this condition as the concentration increases. A more restrictive condition for eqn. 10, that the mean scattering length is larger than the length of structural correlations, $l \gg 2a$, is also valid for the range of concentrations and refractive indices considered here. However, Kaplan *et al.* [23] note that this condition may, in fact, be too restrictive based on the results of measurements in highly concentrated suspensions [24–26].

B. Scatterer form factor

The form factor $P(qa)$ accounts for the anisotropy of scattered light. Here, we calculate it by averaging the parallel i_1 and perpendicular i_2 polarization scattering intensities

$$P(qa) = \frac{i_1 + i_2}{2} \tag{11}$$

We calculate i_1 and i_2 using Rayleigh-Gans-Debye (RGD) scattering theory when conditions of weak scattering $|m-1| \ll 1$ and the Born approximation $k_0 a |m-1| \ll 1$ hold. The perpendicular scattering intensity is

$$i_2 = \frac{k_0^6 V^2}{4\pi^2} (m-1)^2 \left\{ \frac{3}{qa^3} (\sin q - q\cos q) \right\}^2 \tag{12}$$

and the parallel intensity

$$i_1 = i_2 \cos^2\theta. \tag{13}$$

$V = \frac{4}{3}\pi a^3$ is the scatterer volume.

For scatterers of any size and refractive index where the limits of RGD theory do not apply, the form factor can be calculated by Mie scattering theory [27], following the method outlined by Kerker [28] and van de Hulst [29]. The perpendicular and parallel scattering intensities are calculated from the corresponding Mie scattering amplitude functions by

$$\begin{aligned} i_1 &= S_1^* S_1 \\ i_2 &= S_2^* S_2 \end{aligned} \tag{14}$$

where

$$S_1(\theta) = \sum_{n=1}^{\infty} \frac{(2n+1)}{n(n+1)}[a_n \pi_n(\cos\theta) + b_n \tau_n(\cos\theta)]$$
$$S_2(\theta) = \sum_{n=1}^{\infty} \frac{(2n+1)}{n(n+1)}[b_n \pi_n(\cos\theta) + a_n \tau_n(\cos\theta)] \quad (15)$$

The Mie coefficients a_n and b_n are defined as

$$a_n = \frac{\psi_n'(mx)\psi_n(x) - m\psi_n(mx)\psi_n'(x)}{\psi_n'(mx)\zeta_n(x) - m\psi_n(mx)\zeta_n'(x)}$$
$$b_n = \frac{m\psi_n'(mx)\psi_n(x) - \psi_n(mx)\psi_n'(x)}{m\psi_n'(mx)\zeta_n(x) - \psi_n(mx)\zeta_n'(x)} \quad (16)$$

where $\psi_n(x)$ (commonly S_n) and $\zeta_n(x)$ are the Riccati-Bessel functions and $x = 2\pi a/\lambda$ is a dimensionless size parameter (λ is the wavelength of the light in the medium). The angular functions $\pi_n(\cos\theta)$ and $\tau_n(\cos\theta)$ equal

$$\pi_n(\cos\theta) = \frac{\mathrm{d}P_n(\cos\theta)}{\mathrm{d}\cos\theta}$$
$$\tau_n(\cos\theta) = \cos\theta \cdot \pi_n(\cos\theta) - \sin^2\theta \frac{\mathrm{d}\pi_n(\cos\theta)}{\mathrm{d}\cos\theta} \quad (17)$$

where $P_n(\cos\theta)$ is the Legendre polynomial. of degree n and $P_n^m(\cos\theta)$ is the associated Legendre polynomial of degree n and order m. The angular functions are numerically implemented using the recursive relation described by Kerker [28]

$$\pi_n'(\cos\theta) = (2n-1)\pi_{n-1}(\cos\theta) + \pi_{n-2}'(\cos\theta) \quad (18)$$

with initial conditions

$$\pi_0'(\cos\theta) = 0$$
$$\pi_1'(\cos\theta) = 0. \quad (19)$$

C. Structure Factor

The structure factor $S(q)$ accounts for the spatial distribution of scatterers and depends on the particle interactions. For calculations with hard spheres, we use the analytic solution for $S(q)$ derived from the Ornstein-Zernike equation with the Percus-Yevick closure [30–33]. Expressions for $S(q)$ are summarized in appendix A.

The hard sphere model is modified to account for electrostatic double-layer interactions using an excluded annulus of radius a_e larger than the physical scatterer radius a when calculating $S(q)$. The form factor is still a function of the physical radius a.

In the case of the attractive interaction, we use a square well interparticle potential

$$\phi(r) = \begin{cases} \infty & r \le 2a \\ -u_0 & 2a < r \le 2(a+\Delta) \\ 0 & 2(a+\Delta) < r \end{cases} \quad (20)$$

where u_0 is the well depth and Δ is the well width. This sticky hard sphere (SHS) model was originally solved by Baxter [34] for an infinitely deep and narrow well. Menon et al. [35] provide a structure factor for a given (square) well depth and width, parameterized by a perturbation parameter $\epsilon = \Delta/(2a+\Delta)$ and a stickiness parameter [34, 36]

$$\tau = (12\epsilon)^{-1} \exp(-u_0/k_B T). \quad (21)$$

Here, the parameters ϵ and u_0 (and thus τ) are chosen to remain above the critical point of the (metastable) binodal at $\tau_c \approx 0.10 - 0.12$ [35–37]. The parameters cover regions both above and below the dynamic percolation line according to the phase diagram of Miller and Frenkel [37]. We summarize the analytic expression for $S(q)$ in appendix B.

III. RESULTS AND DISCUSSION

In the following discussion, we calculate l^* for silica dispersions using eqn. 10. The model parameters are based on experimental values for Stöber silica particles. The refractive index is $n_p = 1.447$ [38–40], the solvent refractive index $n_s = 1.333$, and the light vacuum wavelength $\lambda = 685$ nm. The magnitudes of the calculated l^* for both repulsive and attractive suspensions are sensitive to the particle and solvent refractive indexes. When using the value $n_p = 1.457$, for instance, the magnitudes of the l^* can differ by approximately 25%. We first discuss the effect of repulsive interactions on l^*, then we turn to attractive interactions.

A. Repulsive interactions

We plot l^* for silica particles with $a = 172.5$ nm in Fig. 1a. As expected, l^* decreases with increasing scatterer concentration. Below volume fractions $\phi < 0.08$, l^* is fairly insensitive to the particle interactions. Above this concentration, interactions between particles, either from the excluded volume of hard spheres or an excluded annulus, lead to modestly higher l^* values compared to the case where interactions are neglected (using $S(q) = 1$ in eqn. 10). Note that the excluded annulus is not considered as a physical layer of the particle, so it does not contribute to the calculations for volume fraction nor the form factor.

On the same figure, experimental measurements of l^* are shown for monodisperse silica particles with diameter $2a = 345$ nm. The experiments for determining the l^* use the transmittance method [41] where the transmittance intensity is measured and compared with that from a standard sample with known l^*,

$$l^* = \frac{T}{T_{\mathrm{ref}} + 4l^*_{\mathrm{ref}}/3L(T_{\mathrm{ref}} - T)} l^*_{\mathrm{ref}} \quad (22)$$

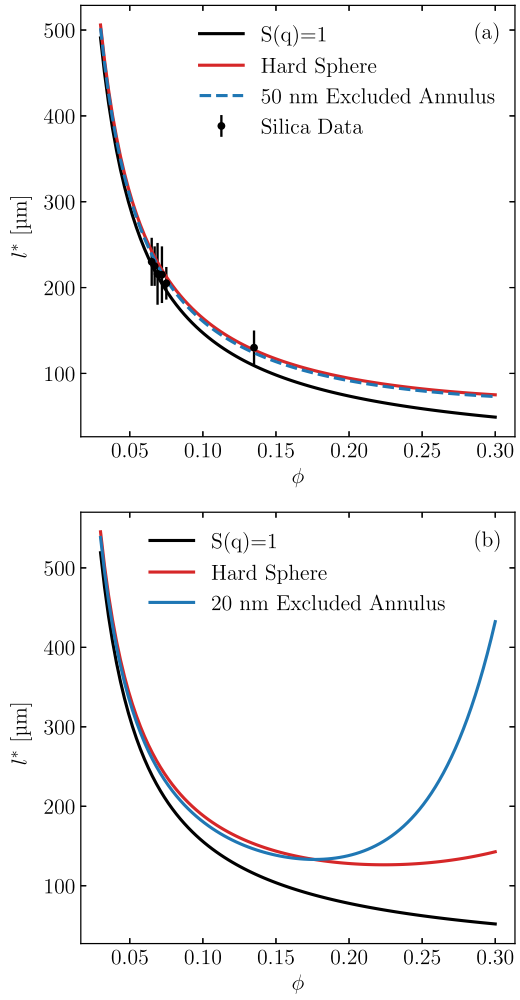

FIG. 1. The transport mean free path, l^*, as a function of volume fraction for the aqueous silica with (a) $a = 172.5$ nm, and (b) $a = 100$ nm.

where T and T_{ref} indicate the transmittance intensity. L is the sample or cuvette thickness, and l^*_{ref} is the known value of the standard sample. The transmittance intensities were measured using DWS RheoLab (LS Instruments AG, Fribourg, Switzerland). From Figure 1a, we find that the experimentally measured l^* values agree with calculated l^* when the excluded annulus is considered. There is good agreement when we use an excluded annulus of ~ 50.0 nm, which is close to the Debye length of the suspension.

A more interesting case occurs when we calculate l^* for smaller particles (less than half the size) with radius $a = 100$ nm (Fig. 1b). At low volume fractions, the photon mean-free path length does not depend significantly on the interactions, but its value is slightly larger than that in Fig. 1a owing to the weaker scattering of the smaller particles. With increasing concentration, however, the smaller particles exhibit a larger difference between l^* values for hard spheres than when we neglect

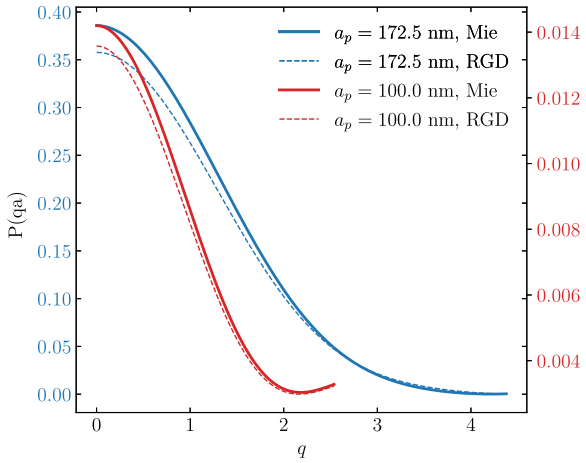

FIG. 2. Form factor, $P(qa)$, as a function of the normalized wave vector, qa, for silica of two sizes (in radius): 172.5 nm (blue curve, left axis) and 100 nm (red curve, right axis) dispersed in water. The $P(qa)$s calculated from different theories (RGD and Mie) are also compared.

interactions. More surprising, though, is the effect when a modest excluded annulus of 20 nm is added. This repulsion leads to strong non-monotonic behavior in l^*. The values first decrease, then rise steeply for volume fractions above approximately $\phi > 0.15$. To explain these results, we next will examine the form factor and structure factors of the scatterers that lead to the l^* values shown in Fig. 1.

The form factors $P(q)$ calculated from RGD and Mie theories are compared in Fig. 2 for the two particle sizes. Each curve is plotted between $0 \leq q \leq 2k_0$ to be consistent with the upper integration limit in eqn. 10. As expected, the form factor decreases markedly with increasing scattering vector. The smaller particles begin to exhibit an upturn before the cutoff.

Examining Fig. 2, we see that increasing particle size leads to more light scattered in the forward direction. $P(qa)$ scales with the square of the particle volume, $P(0) \approx 4\pi\Delta\rho^2 V^2$, where $\Delta\rho$ is the difference in scattering density between particle and surrounding. Therefore, $P(qa)$ for the 100 nm radius particles is approximately 25 times smaller than the values for 172.5 nm nanometer radius particles. For silica particles, the RGD approximation is in relatively good agreement with Mie theory, with smaller values in the low-qa regime. Although we use Mie scattering in this work, it is useful to see that reasonable results can be obtained with the simpler analytic theory when its conditions are met.

While the form factor features (and magnitudes) provide scattering information of single particle, and are important in determining l^*, the structure factor, $S(q)$, reveals the characteristics of inter-particle scattering effects. A representative set of $S(qa)$ curves for aqueous silica with a diameter of $2a = 345$ nm at three selected volume fractions are presented in Fig. 3a. Similar to

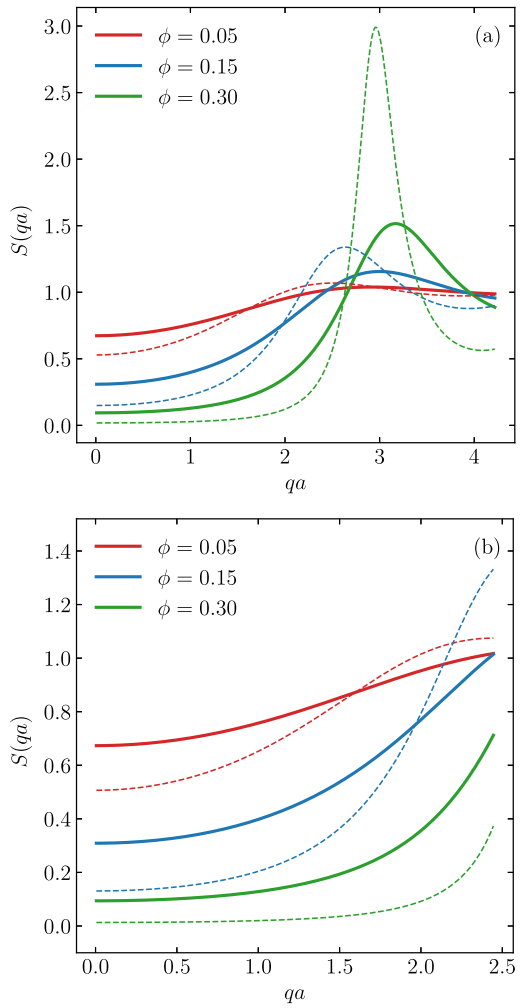

FIG. 3. Structure factor as a function of qa for a model repulsive hard-sphere silica system (solid lines) with different volume fractions: 0.05, 0.15, and 0.30 for particle radii (a) $a = 172.5$ nm and (b) $a = 100$ nm. The dashed lines represent calculations with an excluded annulus thickness of 30 nm.

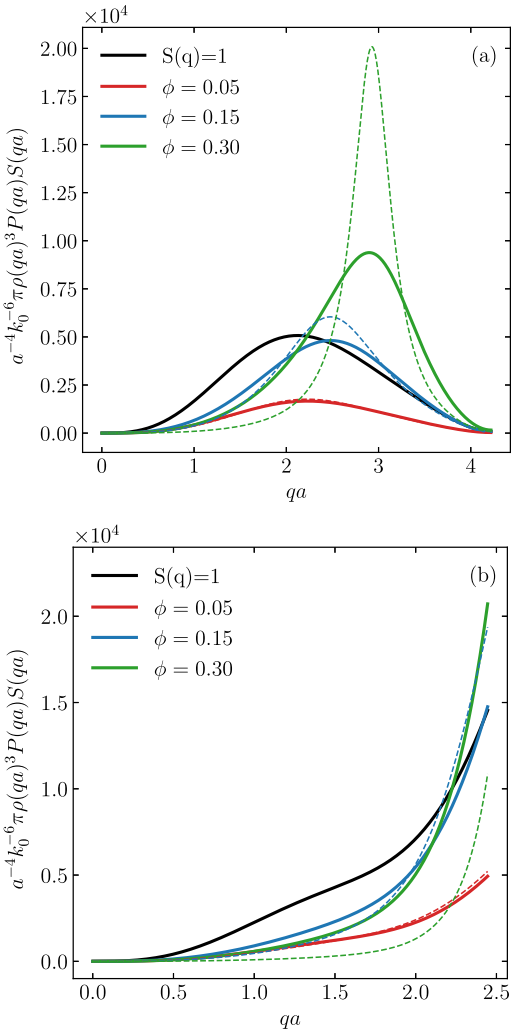

FIG. 4. The integrand, $a^{-4}k_0^{-6}\pi\rho(qa)^3P(qa)S(qa)$, as a function of qa for repulsive suspensions (a) of three different volume fractions and with an excluded annulus $a_e = 30$ nm, and (b) when the particle radius is smaller, $a = 100$ nm.

Fig. 2 the curves are plotted to a scaled scattering vector magnitude $qa = 2k_0a$.

In this range of scattering vectors, the structure factor exhibits modest variations at $\phi = 0.05$. The magnitude of the variation increases with volume fraction and the major peak in $S(qa)$ shifts toward high-qa values with increasing volume fraction. In the low-q regime, $S(qa)$ decreases over the same concentrations. The magnitude of both of these changes is larger when an excluded annulus is included, representing the larger effective repulsion due to the electrostatic double layer, and the higher *effective* (not solids) volume fraction of the suspension.

For larger scatterers, significant features of the structure factor stay within the range of scattering angles accessible in a DWS experiment. As particles become smaller, the case becomes different (Fig. 3b). The peak of the structure factor now lies outside of the range of scattering vectors. As the concentration increases, the magnitude of $S(qa)$ monotonically decreases. In both cases of physical (hard sphere) and effective (with excluded annulus) volume fractions, the limiting values of $S(0)$ agree with the Carnahan-Starling expression [42]

$$S(0) = \frac{(1-\phi)^4}{(1+2\phi)^2 + \phi^3(\phi-4)} \tag{23}$$

Now the behavior of l^* for repulsive interactions with different scatterer sizes can be understood by examining the contributions of $P(qa)$ and $S(qa)$ in eqn. 10. We plot the integrand, $a^{-4}k_0^{-6}\pi\rho(qa)^3P(qa)S(qa)$, in Fig. 4, which accounts for the form and structure factor as well as the q^3 weighting. For larger particles (Fig. 4a), the integrand values stay nearly entirely within the range $0 \leq qa \leq 2k_0$, with a maximum observed. While an

excluded annulus leads to a higher peak, the change in the total area is limited due to the mass conservation in the scattering vector space. For smaller particles (Fig. 4b), the integrand curves increase from $\phi = 0.05$ to 0.15, then essentially remain unchanged to $\phi = 0.3$. However, the excluded annulus causes the integrand to drop significantly at the higher concentration, which leads to the large increase in l^*.

Our analysis leads to a general heuristic for DWS experiments to account for possible changes in l^* with increasing concentration: if the particle radius is sufficient large such that the maximum of the structure factor $S(q_{\max})$ remains within $0 \leq q_{\max}a \leq 2k_0a$, then l^* will track with values where interactions are neglected. A reasonable approximation (for spherical scatterers) is to use the hard sphere structure factor. If, however, $q_{\max}a > 2k_0a$, since $q_{\max} \sim \pi/a$, scatterers with diameters

$$2a < \lambda/2n_s \tag{24}$$

could exhibit strong non-monotonic behavior of l^* with increasing concentration.

B. Attractive Suspensions

Knowing the importance of repulsive interactions and suspension structure in the l^* calculation, we extend our analysis to attractive interactions using the sticky hard sphere model (SHS). Based on the phase diagram of the SHS particles [35, 43], three sets of model parameters are chosen to examine three different points in the phase diagram: the liquid state ($\tau = 0.40$, $\epsilon = 0.10$, $\eta = \phi/(1-\epsilon)^3 = 0.21$), on the dynamic percolation line ($\tau = 0.15$, $\epsilon = 0.02$, $\eta = \phi/(1-\epsilon)^3 = 0.16$), and below the percolation line ($\tau = 0.15$, $\epsilon = 0.02$, $\eta = \phi/(1-\epsilon)^3 = 0.32$).

Attractive interactions in suspensions have a significant effect on the structure factor, mainly as an increase at low scattering vectors. Low-q upturns indicate large scale structures formed within the suspension [44–46]. These signatures are clearly visible in fig. 5 for both particle sizes. Here, the structure factor $S(q)$ in the low-q regime has the largest values close to the percolation line. $S(q)$ is not only affected by the attractive interaction, but also by the volume fraction. Furthermore, while the major $S(q)$ peaks are not captured for smaller particles, same as what was seen in repulsive suspensions, the low-q behavior is less sensitive to particle size.

Even with significant differences between repulsive and attractive structure in the low-q regime, its effect on the integrand of eqn. 10, and hence on light transport, is weak (Fig. 6). The shapes and characteristics of the integrand are qualitatively similar to the results for repulsive particles (Fig. 4), mainly due to the q^3 weighting in eqn. 8. For smaller particles, the shape is insensitive to differences in the attractive interaction. Moreover, while the excluded annulus in repulsive systems compresses the shape of the

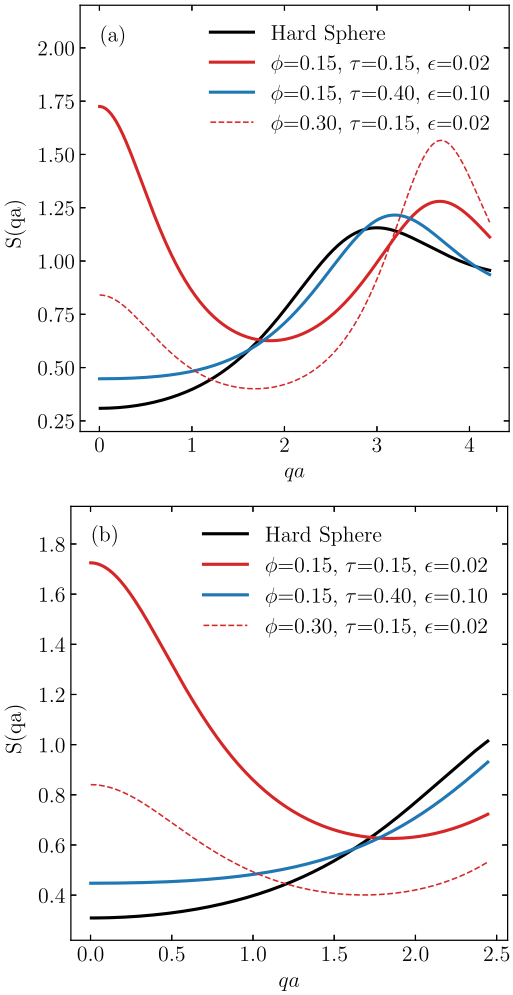

FIG. 5. Structure factor as a function of qa for a model attractive silica system with different volume fractions: 0.05, 0.15, and 0.30. Calculations for two particle radii are shown: (a) $a = 172.5$ nm and (b) $a = 100$ nm.

peaks of the integrand, the attractive interaction effectively shifts the location of peaks in the qa dimension.

The calculated l^* values as a function of volume fraction of the attractive suspensions are presented in Fig. 7. For both particle sizes, the l^* values are close to those for repulsive suspensions. However, for smaller particles, when the liquid state example shows the l^* upturn above around $\phi = 0.15$, the introduction of attractive interaction effectively suppresses this. At relatively high volume fractions, the excluded annulus "compresses" the first peak of $S(q)$, bringing the integrand to a lower value shown in Fig. 7b, while this is not observed in attractive suspensions (Fig. 7b).

We measured l^* for the same silica suspension used above with addition of 120 mM sodium chloride to introduce a weak attraction. Based on the expected van der Waals and double layer interactions (Hamaker constant

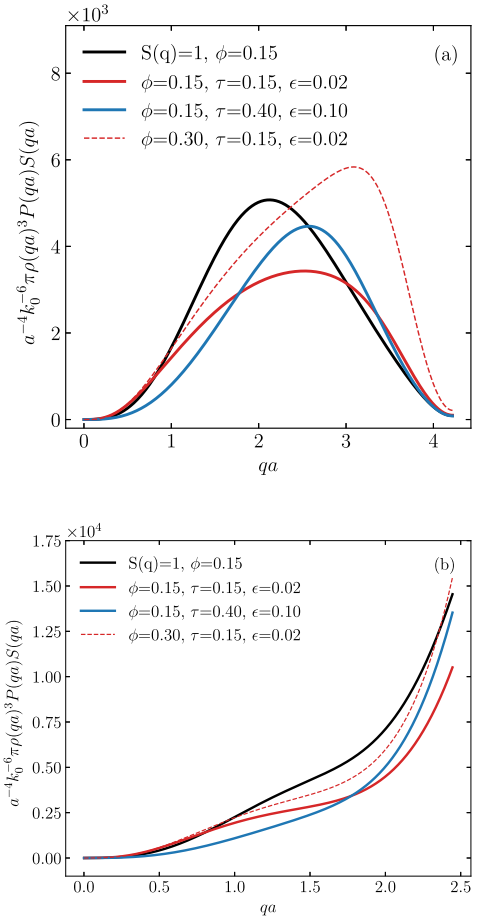

FIG. 6. The integrand, $a^{-4}k_0^{-6}\pi\rho(qa)^3P(qa)S(qa)$, as a function of qa for attractive aqueous silica suspensions with two radii: (a) $a = 172.5$ nm and (b) $a = 100$ nm.

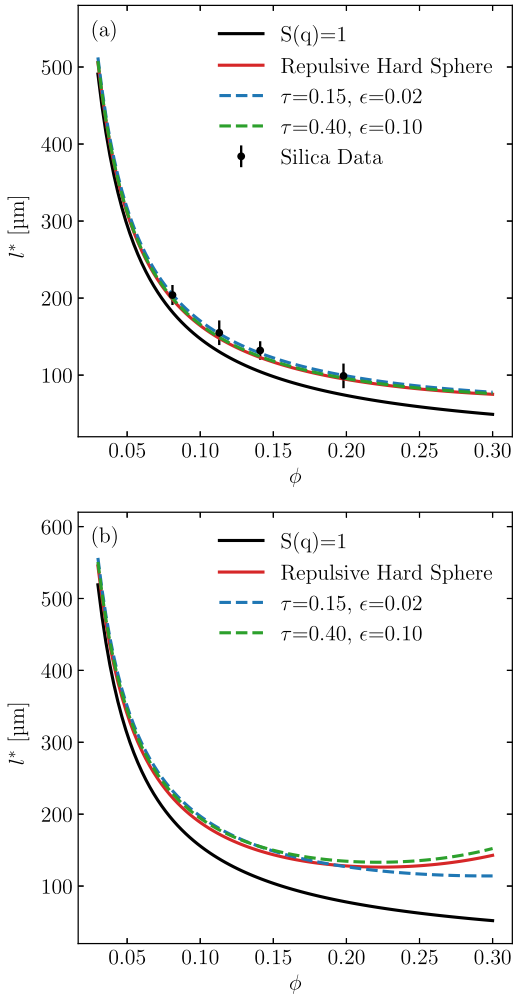

FIG. 7. The transport mean free path, l^*, as a function of volume fraction for attractive aqueous silica suspensions with two different sizes: (a) $a = 172.5$ nm, (b) $a = 100$ nm.

$A_H = 0.83 \times 10^{-21}$ J, surface potential $\psi_0 = -40$ mV), this should lead to a secondary minimum in the interaction potential on the order of 2-3 kT and range $\Delta \sim 10$ nm. The results of the measurements agree well with the calculations (Fig. 7a).

IV. CONCLUSION

In this work, we examined the effect of particle interactions on the light transport properties of suspensions. In repulsive suspensions, l^* is calculated with hard sphere and excluded annulus interactions. The values of l^* for larger scatterers agree with experimental measurements. However, when the particle size is sufficiently small compared with the light wavelength, l^* may change non-monotonically with increasing volume fraction. This is explained by the range of accessible scattering vectors, $0 \leq qa \leq 2k_0a$. For smaller particles, the first peak of the structure factor $S(q)$ exceeds $2k_0$; the particles are crowded together and scattering is dominated by lower wavevectors, which decrease with increasing concentration. This is, in part, why applications such as opacifiers in coatings require the particle sizes to be on the order of half the wavelength.

The effect of attractive suspensions were modeled with the sticky hard sphere model (SHS) using the solutions developed by Menon et al. [35]. While we might expect to see significant effects on l^* with attraction due to changes in the structure factor, the fact that these occur at low wavevectors, combined with the strong weighting of eqn. 10 to higher q, makes the light transport properties relatively insensitive to the presence of attraction. However, the current work focuses on situations where the attraction is sufficiently weak that phase separation or gelation do not occur. In the latter case, the strong particle localization will affect the scattering form and structure factors, potentially through strong resonant scattering between particles.

These results give DWS users greater confidence that

the light transport properties can be separated from changes in the dynamics measured using diffusing wave spectroscopy, and provide important guidance for the interpretation of experiments when using particles that are small relative to the wavelength of light. In situations where strong particle localization occurs, close to maximum packing or in a gel, the particle scattering and light transport models used here may not apply. However, the results of this work are useful for cases when DWS is used to characterize particle interactions and their effect on suspension dynamics at moderate volume fractions.

V. ACKNOWLEDGMENTS

This research was primarily supported by NSF through the University of Delaware Materials Research Science and Engineering Center DMR-2011824. Additional financial support was received from the Chemours Company, Wilmington, DE.

Appendix A: Percus-Yevick structure factor

The Percus-Yevick (PY) closure of the Ornstein-Zernicke integral equation yields an analytic expression for the structure factor, [30, 33] which is related to the Fourier transform of the direct correlation function $\hat{C}(q)$ by

$$S(q) = \frac{1}{1-\rho\hat{C}(q)}. \tag{A1}$$

With the parameters

$$\lambda_1 = \frac{(1+2\phi)^2}{(1-\phi)^4} \tag{A2}$$

and

$$\lambda_2 = \frac{-(1+\phi/2)^2}{(1-\phi)^4} \tag{A3}$$

where ρ is the density of the scattering particle. ϕ is the volume fraction. The Fourier transform of the direct correlation function is

$$\rho\hat{C}(q) = -24\phi(c_1+c_2+c_3) \tag{A4}$$

where

$$c_1 = \frac{\lambda_1}{(2qa)^3}\left[\sin(2qa) - (2qa)\cos(2qa)\right], \tag{A5}$$

$$\begin{aligned} c_2 =& \frac{-6\phi\lambda_2}{(2qa)^4}\left[(2qa)^2\cos(2qa)\right. \\ & \left. -2(2qa)\sin(2qa) - 2\cos(2qa) + 2\right], \end{aligned} \tag{A6}$$

and

$$\begin{aligned} c_3 =& \frac{-\phi\lambda_1/2}{(2qa)^6}\left[(2qa)^4\cos(2qa)\right. \\ & -4(2qa)^3\sin(2qa) - 12(2qa)^2\cos(2qa) \\ & \left. +24(2qa)\sin(2qa) + 24\cos(2qa) - 24\right]. \end{aligned} \tag{A7}$$

The PY solution overestimates the packing density of hard spheres near close-packing by a factor $3\sqrt{2}/\pi$ [33] and for $\phi = 0.3$ the PY theory gives a value for the osmotic compressibility $S(0)$ that is 4% too low [47]. For our purposes, at volume fractions far from close-packing and where the q^3 dependence of multiple scattering weights higher scattering vectors, the analytic form and reasonable accuracy of the PY model justify its use.

Appendix B: Sticky hard sphere structure factor

The structure factor for sticky hard spheres is expressed in the form [35]

$$S(q) = \frac{1}{A^2(q) + B^2(q)} \tag{B1}$$

where

$$\begin{aligned} A(q) = 1 + 12\eta\Big\{&\alpha\Big[\frac{\sin(q)-\kappa\cos(q)}{\kappa^3}\Big] \\ &+\beta\Big[\frac{1-\cos(\kappa)}{\kappa^2}\Big] - \frac{\lambda}{12}\frac{\sin(q)}{\kappa}\Big\} \end{aligned} \tag{B2}$$

$$\begin{aligned} B(q) = 12\eta\Big\{&\alpha\Big[\frac{1}{2\kappa} - \frac{\sin(\kappa)}{\kappa^2} + \frac{1-\cos(\kappa)}{\kappa^3}\Big] \\ &+\beta\Big[\frac{1}{\kappa} - \frac{\sin(\kappa)}{\kappa^2}\Big] - \frac{\lambda}{12}\Big[\frac{1-\cos(\kappa)}{\kappa}\Big\} \end{aligned} \tag{B3}$$

and

$$\begin{aligned} \kappa &= qa \\ \eta &= \frac{\phi}{(1-\epsilon)^3} \\ \alpha &= \frac{1+2\eta-\mu}{(1-\eta)^2} \\ \beta &= \frac{-3\eta+\mu}{2(1-\eta)^2}, \quad \mu = \lambda\eta(1-\eta) \end{aligned} \tag{B4}$$

where λ can be solved using the quadratic

$$\lambda\tau = \frac{1+\eta/2}{(1-\eta)^2} - \frac{\lambda\eta}{(1-\eta)} + \frac{\lambda^2\eta}{12}. \tag{B5}$$

Appendix C: Python code

An open-access Python code [22] is available for estimating the light transport properties in DWS microrheology. The modular structure of the Python compilation

enables the customization of the form factor and structure factor models in scattering, and the applications on various of colloidal systems.

The main file is `scattering.py`. The functions `mie_scattering` and `rayleigh_scattering` calculate light scattering properties for scatterers, including scattering intensities and photon mean-free path. The input parameters are the particle and medium refractive indices, particle radius, and incident light wavelength along with the desired structure factor model. The default is to assume non-interacting particles by setting the structure factor $S(q) = 1$. The documentation within `scattering.py` provides further details. Examples calculations and scripts can be found in the repository.

[1] D. J. Pine, D. A. Weitz, P. M. Chaikin, and E. Herbolzheimer, Phys. Rev. Lett. **60**, 1134 (1988).
[2] D. Weitz and D. Pine, Brown W, New York: Oxford University Press **16**, 652 (1993).
[3] H. M. Wyss, S. Romer, F. Scheffold, P. Schurtenberger, and L. J. Gauckler, J Colloid Interface Sci. **240**, 89 (2001).
[4] L. Rojas-Ochoa, S. Romer, F. Scheffold, and P. Schurtenberger, Phys. Rev. E **65**, 051403 (2002).
[5] Z. Gaygadzhiev, M. Corredig, and M. Alexander, Langmuir **24**, 3794 (2008).
[6] Q. Li, X. Peng, and G. B. McKenna, Soft Matter **13**, 1396 (2017).
[7] H. S. Kim, N. Şenbil, C. Zhang, F. Scheffold, and T. G. Mason, Proc. Natl. Acad. Sci. USA **116**, 7766 (2019).
[8] Y. Xu, F. Scheffold, and T. G. Mason, Phys. Rev. E **102**, 062610 (2020).
[9] J. G. Wang, Q. Li, X. Peng, G. B. McKenna, and R. N. Zia, Soft matter **16**, 7370 (2020).
[10] Q. Lu and M. J. Solomon, Phys. Rev. E **66**, 061504 (2002).
[11] A. Matsumoto, C. Zhang, F. Scheffold, and A. Q. Shen, ACS Macro Letters **11**, 84 (2021).
[12] M. Alexander and D. G. Dalgleish, Langmuir **21**, 11380 (2005).
[13] M. Panouillé, D. Durand, T. Nicolai, E. Larquet, and N. Boisset, J. Colloid Interface Sci. **287**, 85 (2005).
[14] A. Niederquell, A. C. Völker, and M. Kuentz, Intl. J. Pharma. **426**, 144 (2012).
[15] A. Mohammed, J. Zurek, S. Madueke, H. Al-Kassimy, M. Yaqoob, C. Houacine, A. Ferraz, R. Kalgudi, M. G. Zariwala, N. Hawkins, *et al.*, Pharm. Res. **37**, 1 (2020).
[16] P. Zakharov and F. Scheffold, Soft Materials **8**, 102 (2010).
[17] T. G. Mason and D. A. Weitz, Phys. Rev. Lett. **74**, 1250 (1995).
[18] T. G. Mason, H. Gang, and D. A. Weitz, J. Opt. Soc. Amer. A **14**, 139 (1997).
[19] E. M. Furst and T. M. Squires, *Microrheology* (Oxford University Press, 2017).
[20] C. J. Kloxin and J. H. van Zanten, Macromolelcules **43**, 2084 (2010).
[21] K. A. Dennis, Y. Gao, A. Phatak, P. F. Sullivan, and E. M. Furst, J. Rheol. **64**, 205 (2020).
[22] https://github.com/emfurst/DWS-interactions (2022).
[23] P. D. Kaplan, A. D. Dinsmore, A. G. Yodh, and D. J. Pine, Phys. Rev. E **50**, 4827 (1994).
[24] S. Fraden and G. Maret, Phys. Rev. Lett. **65**, 512 (1990).
[25] X. Qiu, X. L. Wu, J. Z. Xue, D. J. Pine, D. A. Weitz, and P. M. Chaikin, Phys. Rev. Lett. **65**, 516 (1990).
[26] J.-Z. Xue, X.-L. Wu, D. J. Pine, and P. M. Chaikin, Phys. Rev. A **45**, 989 (1992).
[27] G. Mie, Annalen der Physik **330**, 377 (1908).
[28] M. Kerker, *The Scattering of Light and Other Electromagnetic Radiation* (Academic Press, New York, 1969).
[29] H. C. van de Hulst, *Light Scattering by Small Particles* (Wiley, New York, 1957).
[30] J. K. Percus and G. J. Yevick, Physical Review **110**, 1 (1958).
[31] J. Perram, Mol. Phys. **30**, 1505 (1975).
[32] A. Vrij, J. Chem.. Phys. **71**, 3267 (1979).
[33] M. Wertheim, Phys. Rev. Lett. **10**, 321 (1963).
[34] R. Baxter, J. Chem.. Phys. **49**, 2770 (1968).
[35] S. Menon, C. Manohar, and K. S. Rao, J. Chem.. Phys. **95**, 9186 (1991).
[36] M. G. Noro and D. Frenkel, J. Chem. Phys. **113**, 2941 (2000).
[37] M. A. Miller and D. Frenkel, J. Chem. Phys. **121**, 535 (2004).
[38] F. Garcia-Santamaria, H. Miguez, M. Ibisate, F. Meseguer, and C. Lopez, Langmuir **18**, 1942 (2002).
[39] B. N. Khlebtsov, V. A. Khanadeev, and N. G. Khlebtsov, Langmuir **24**, 8964 (2008).
[40] G. J. Ojeda-Mendoza, H. Contreras-Tello, and L. F. Rojas-Ochoa, Coll. Surf. A: Physicochemical and Engineering Aspects **538**, 320 (2018).
[41] P. Kaplan, M. H. Kao, A. Yodh, and D. J. Pine, Applied Optics **32**, 3828 (1993).
[42] N. F. Carnahan and K. E. Starling, J. Chem.. Phys. **51**, 635 (1969).
[43] Y. Chiew and E. Glandt, J. Phys. A: Mathematical and General **16**, 2599 (1983).
[44] C. J. Dibble, M. Kogan, and M. J. Solomon, Phys. Rev. E **74**, 41403 (2006).
[45] N. E. Valadez-Pérez, Y. Liu, A. P. Eberle, N. J. Wagner, and R. Castaneda-Priego, Phys. Rev. E **88**, 060302 (2013).
[46] K. A. Whitaker, Z. Varga, L. C. Hsiao, M. J. Solomon, J. W. Swan, and E. M. Furst, Nature communications **10**, 1 (2019).
[47] J.-P. Hansen and I. R. McDonald, *Theory of Simple Liquids*, 2nd ed. (Academic Press, New York, 1992).